Available online at www.sciencedirect.com
ScienceDirect
Ceramics International 37 (2011) 2489–2493
CERAMICS INTERNATIONAL
www.elsevier.com/locate/ceramint

Preparation and thermophysical properties of $LaMgAl_{11}O_{19}$–$Yb_3Al_5O_{12}$ ceramic composites

Yuan-Hong Wang, Zhan-Guo Liu, Jia-Hu Ouyang *, Hong-Zhi Liu, Ren-Xian Zhu

School of Materials Science and Engineering, Harbin Institute of Technology, No. 92 West Da-Zhi Street, Harbin 150001, China

Received 13 January 2011; received in revised form 26 March 2011; accepted 29 March 2011
Available online 8 April 2011

Abstract

$LaMgAl_{11}O_{19}$–$Yb_3Al_5O_{12}$ ceramic composites were prepared by pressureless sintering process at 1700 °C for 10 h in air. The microstructure and thermophysical properties of the composites were characterized by X-ray diffraction, scanning electron microscopy, high-temperature dilatometer and laser flash diffusivity measurements. $LaMgAl_{11}O_{19}$–$Yb_3Al_5O_{12}$ ceramic composites are composed of magnetoplumbite and garnet structures. $LaMgAl_{11}O_{19}$–$Yb_3Al_5O_{12}$ ceramic composites exhibit typical linear increase in thermal expansion with the increase of temperature. The measured thermal diffusivity gradually decreases with increasing temperature. Thermal conductivity of $LaMgAl_{11}O_{19}$–$Yb_3Al_5O_{12}$ ceramic composites is in the range of 2.6–3.9 $W{\cdot}m^{-1}{\cdot}K^{-1}$ from room temperature to 1200 °C.

Keywords: $LaMgAl_{11}O_{19}$; $Yb_3Al_5O_{12}$; Composites; Thermal properties; Thermal applications

1. Introduction

Thermal barrier coatings (TBCs) applied on the surface of hot section in advanced engines are used to protect metallic components from high temperature and environmental corrosion [1–6]. The current state-of-art of TBCs in commercial use is 6–8 wt.% partially yttria-stabilized zirconia (6–8YSZ) due to its low thermal conductivity and high thermal expansion coefficient. However, the widely used YSZ layers are prone to sintering and phase transition at temperatures higher than 1200 °C, which results in the increase of thermal conductivity and less effective use [7,8]. Therefore, it urgently needs to seek new TBCs material instead of the YSZ. Lanthanum hexaaluminte ($LaMgAl_{11}O_{19}$, LHA) with a magnetoplumbite structure is a candidate for TBCs applications [9]. LHA has a crystal habit to platelets, and the magnetoplumbite is known to have a layered structure composed of spinel blocks and conduction layers which are stacked alternately [10]. LHA has a relatively low thermal conductivity due to its crystal structure. As the oxygen conductivity is suppressed along to *c*–axis orientation, the presence of LHA ceramic coating can decrease the oxidation process of the metallic substrate effectively [11]. Rare earth oxides have high melting points, low thermal conductivities and large thermal expansion coefficients. The addition of rare earth oxide into a ceramic material usually results in the decrease of thermal conductivity and the increase of thermal expansion coefficient, which are two very important thermo-physical properties for TBCs materials [3]. It was reported that the doped $Gd_{0.7}Yb_{0.3}MgAl_{11}O_{19}$ composition has a lower thermal conductivity than undoped $GdMgAl_{11}O_{19}$ [12]. YSZ doped with different rare earth oxides of Yb_2O_3, Gd_2O_3, Nd_2O_3, Sm_2O_3 or Er_2O_3 exhibits a low thermal conductivity [13,14]. The similar results were also found in pyrochlore-type rare-earth zirconates doped with rare-earth oxides of Nd_2O_3, Gd_2O_3 or Yb_2O_3 at the rare-earth site [15–17].

In this study, $LaMgAl_{11}O_{19}$–$Yb_3Al_5O_{12}$ ceramic composites were prepared by pressureless sintering process at 1700 °C for 10 h in air. The microstructure and thermo-physical properties of $LaMgAl_{11}O_{19}$–$Yb_3Al_5O_{12}$ ceramic composites were investigated.

2. Experimental

$(1–x)LaMgAl_{11}O_{19} - xYb_3Al_5O_{12}$ ($x = 0$, 0.04, 0.08) ceramic powders were synthesized by the chemical-coprecipitation and calcination method using La_2O_3, Yb_3O_3 (Grirem Advanced

* Corresponding author. Tel.: +86 451 86414291; fax: +86 451 86414291.
E-mail address: ouyangjh@hit.edu.cn (J.-H. Ouyang).

0272-8842/$36.00
doi:10.1016/j.ceramint.2011.03.039

Materials Co. Ltd., China; purity ≥ 99.9%), $Al(NO_3)_3{\cdot}9H_2O$ and $Mg(NO_3)_2{\cdot}6H_2O$ (Tianjin Guangfu Fine Chemical Research Institute. Ltd., China; Analytical pure) powders as raw materials. La_2O_3 and Yb_2O_3 powders were calcined at 900 °C for 2 h in air to remove adsorptive water and carbon dioxide before weighing. La_2O_3 and Yb_2O_3 were weighed and dissolved in dilute nitric acid, while $Al(NO_3)_3{\cdot}9H_2O$ and $Mg(NO_3)_2{\cdot}6H_2O$ were dissolved in de-ionized water. These solutions were mixed, stirred, filtered, and were slowly added under stirring to excessive dilute ammonium hydrate solution to obtain gel-like precipitates. These gels were washed with de-ionized water several times, and were then washed with absolute alcohol twice. The precipitates were dried and then calcined at 800 °C for 5 h in air. The powders were uniaxially pressed into pellets at 20 MPa. The pellets were further compacted by cold isostatic pressing at 280 MPa for 5 min, and then pressureless-sintered at 1700 °C for 10 h in air to obtain dense $LaMgAl_{11}O_{19}$–$Yb_3Al_5O_{12}$ ceramic composites.

The phase constituents of $LaMgAl_{11}O_{19}$–$Yb_3Al_5O_{12}$ ceramic composites were identified by X-ray diffraction (XRD, Rigaku D/Max 2200VPC, Japan) with Cu *K*α radiation. XRD patterns were recorded in a scanning range of 10–70° at room temperature, and a scan rate of 4°/min was employed. The bulk density of cylindrical specimens was measured by the usual volume and weight measurement technique, and the theoretical density of $LaMgAl_{11}O_{19}$–$Yb_3Al_5O_{12}$ ceramic composites was calculated by the mixing rule. Microstructure of $LaMgAl_{11}O_{19}$–$Yb_3Al_5O_{12}$ ceramic composites was observed with a scanning electron microscope (CamScan MX 2600FE, UK), while the local compositions of interest were particularly analyzed with the equipped energy-dispersive X-ray spectroscopy (Oxford Instruments INCA X-sight system, 7537, UK). SEM specimens were prepared by polishing the surface to 1 μm finish, and then by thermally etching at 1600 °C for 1 h in air. A thin gold coating was evaporated onto the surfaces of the specimens for SEM observations.

The thermal diffusivity measurements were carried out using the laser flash technique (Netzsch LFA 427, Germany).The specimens with the size of 12.7 mm in diameter and about 2 mm in thickness were measured in an argon gas atmosphere from room temperature to 1200 °C. The specific heat capacity C_p was calculated from the chemical compositions of composite with the Neumann-Kopp rule [18]. The heat capacity data of each constituent oxide (La_2O_3, Yb_2O_3, MgO and Al_2O_3) was obtained from the literature [19]. Thermal conductivity k of the composite was calculated from heat capacity C_p, density ρ and thermal diffusivity λ, and using the following equation,

$$k = C_p \cdot \rho \cdot \lambda \quad (1)$$

As the composite was not fully dense, the measured thermal conductivity k was corrected for the theoretical thermal conductivity k_0 with residual porosity φ of the samples, using the equation [8]:

$$\frac{k}{k_0} = 1 - \frac{4}{3}\varphi \quad (2)$$

The linear thermal expansion behavior of the composite was studied by a high-temperature dilatometer (Netzsch DIL 402 C, Germany). The thermal expansion of specimens with the dimensions of approximately 2.5 mm × 3.5 mm × 14 mm were measured in an argon atmosphere from 50 °C to 1200 °C at a heating rate of 4 °C/min during heating. The data were corrected by the known thermal expansion of a certified standard alumina.

3. Results and discussion

The XRD patterns of $LaMgAl_{11}O_{19}$–$Yb_3Al_5O_{12}$ ceramic composites sintered at 1700 °C for 10 h in air are shown in Fig. 1. $LaMgAl_{11}O_{19}$ ($x = 0$) has a single magnetoplumbite structure, while the (1–x)$LaMgAl_{11}O_{19}$–$xYb_3Al_5O_{12}$ (x = 0.04, 0.08) ceramic composites are composed of both magnetoplumbite and garnet structures. All the diffraction peaks in Fig. 1 match well with the standard PDF cards of JCPDS 26–0873 and JCPDS 23–1476, respectively. It should be noted that the widening of peak width and peak intensity of most garnet reflexes in the low concentration composite at $x = 0.04$. The relative density of $LaMgAl_{11}O_{19}$–$Yb_3Al_5O_{12}$ ceramic composites sintered at 1700 °C for 10 h in air is over 90%, as shown in Table 1. Fig. 2(a–c) shows the thermally etched morphologies of $LaMgAl_{11}O_{19}$–$Yb_3Al_5O_{12}$ ceramic composites. Clearly, fine $Yb_3Al_5O_{12}$ grains are randomly distributed in the $LaMgAl_{11}O_{19}$ plates. EDS analysis of different phase constituents at different positions of A and B in Fig. 2(b) is shown in Fig. 2(d and e). As shown in Fig. 2(d), the EDS spectrum of the elongated lamellar phase at the position of A only contains La, Mg, Al and O elements. However, the EDS spectrum of very fine particles at the position of B is composed of Yb, Al and O elements as well as La and Mg elements (Fig. 2(e)). Therefore, EDS results of the sample ($x = 0.04$) in Fig. 2(d) indicate that there is no Yb in the $LaMgAl_{11}O_{19}$ phase (labeled as A). However, the garnet phase (labeled as B) in the low

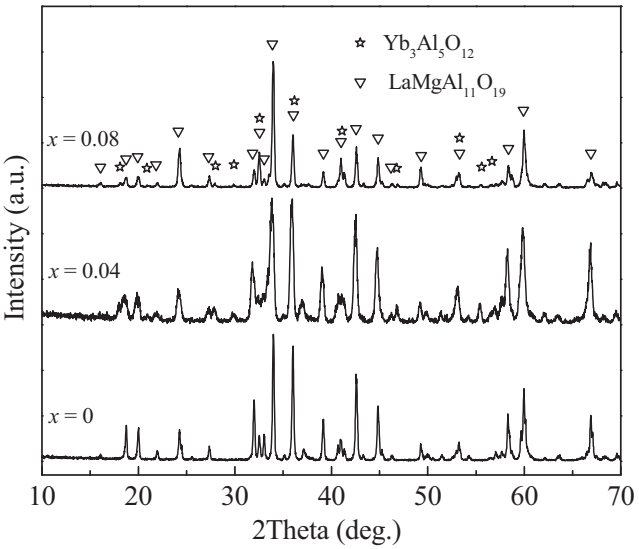

Fig. 1. XRD patterns of $LaMgAl_{11}O_{19}$–$Yb_3Al_5O_{12}$ ceramic composites sintered at 1700 °C for 10 h in air.

Table 1
Relative densities of $LaMgAl_{11}O_{19}$–$Yb_3Al_5O_{12}$ ceramic composites sintered at 1700 °C for 10 h in air.

Ceramics	Relativy density (%)
$LaMgAl_{11}O_{19}$	90.7
$0.96LaMgAl_{11}O_{19}$–$0.04Yb_3Al_5O_{12}$	94.8
$0.92LaMgAl_{11}O_{19}$–$0.08Yb_3Al_5O_{12}$	92.0

concentration composite exhibits a very fine particle incorporated with some LMA composition, and is indicative of incomplete phase separation, which may cause the widening of peak width and strong peak intensity of garnet in the low concentration composite at $x = 0.04$.

The thermal diffusivity of the composite sintered at 1700 °C for 10 h as a function of temperature is shown in Fig. 3. The values in Fig. 3 are the mean values of three measurements of identical ceramic material. The error derived from the mean standard deviation of three measurements for each specimen is less than 1.5%, and the error bars in Fig. 3 are smaller than the symbols. The measured thermal diffusivity of $LaMgAl_{11}O_{19}$–$Yb_3Al_5O_{12}$ ceramic composites decreases with increasing temperature from room temperature to 1200 °C, which is similar to most polycrystalline ceramic materials [20]. The calculated thermal conductivity of $LaMgAl_{11}O_{19}$–$Yb_3Al_5O_{12}$ ceramic composites was corrected to 100% theoretical density according to the Equation (1) and Table 1. The corrected thermal conductivity is plotted as a function of temperature in

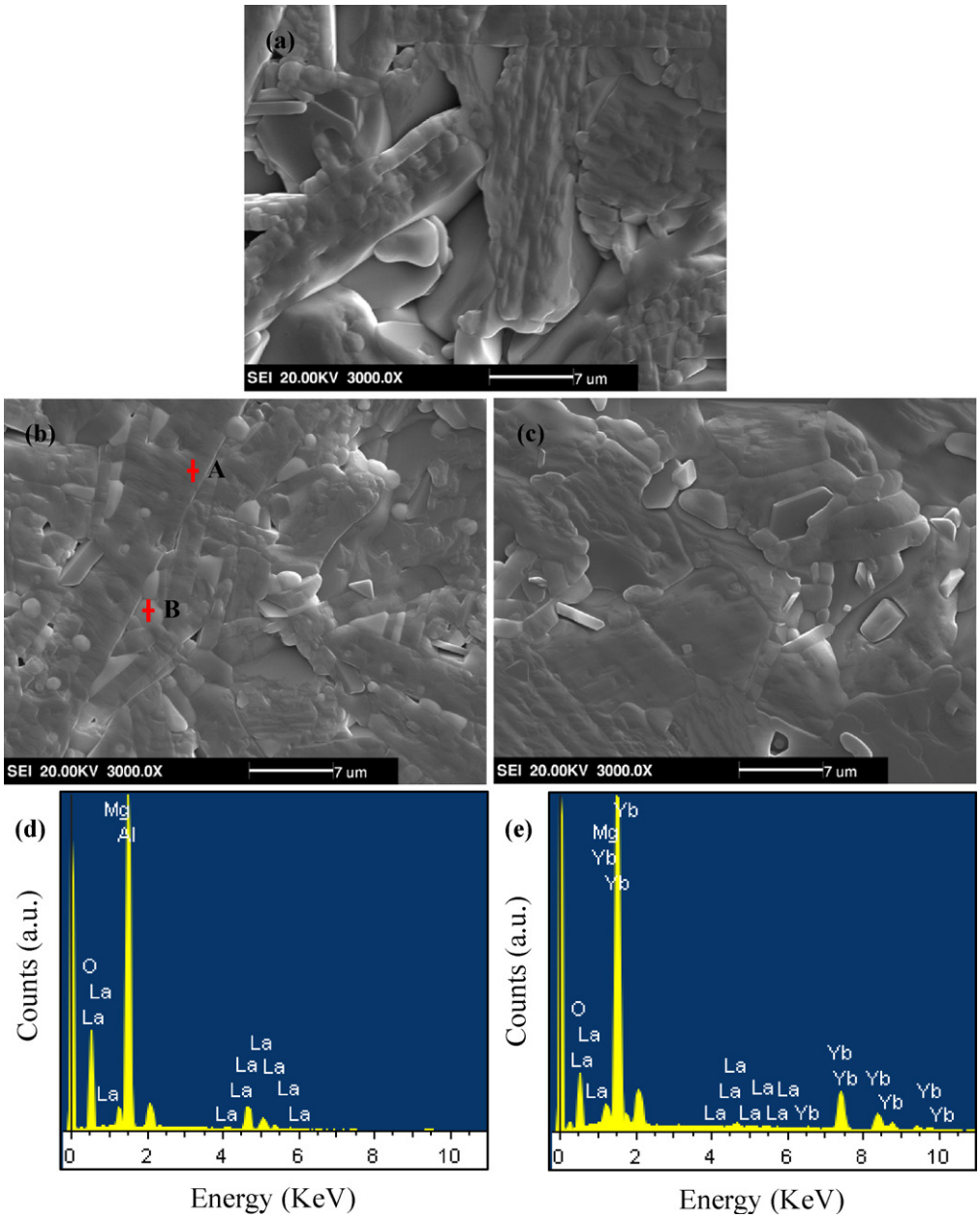

Fig. 2. Microstructure of $LaMgAl_{11}O_{19}$–$Yb_3Al_5O_{12}$ ceramic composites sintered at 1700 °C for 10 h in air: (a) $x = 0$, (b) $x = 0.04$, (c) $x = 0.08$, (d) and (e) EDS spectra at the locations of A and B in (b), respectively.

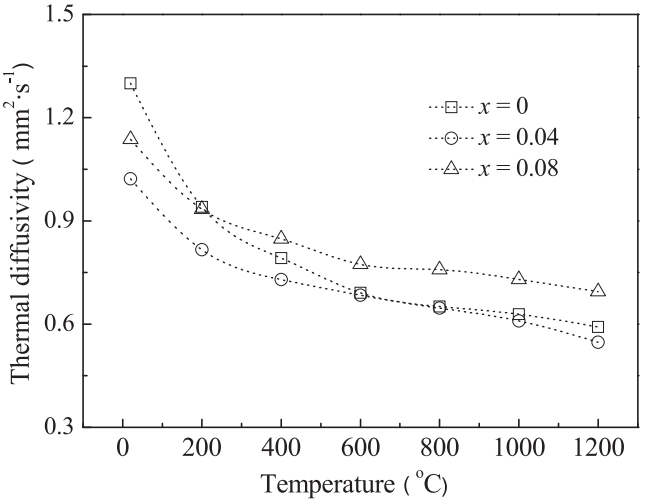

Fig. 3. Thermal diffusivity of $LaMgAl_{11}O_{19}$–$Yb_3Al_5O_{12}$ ceramic composites as a function of temperature.

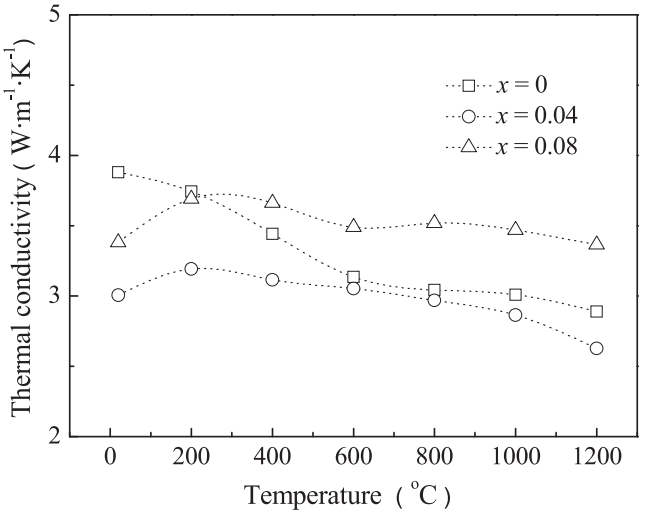

Fig. 4. Thermal conductivity of $LaMgAl_{11}O_{19}$–$Yb_3Al_5O_{12}$ ceramic composites as a function of temperature.

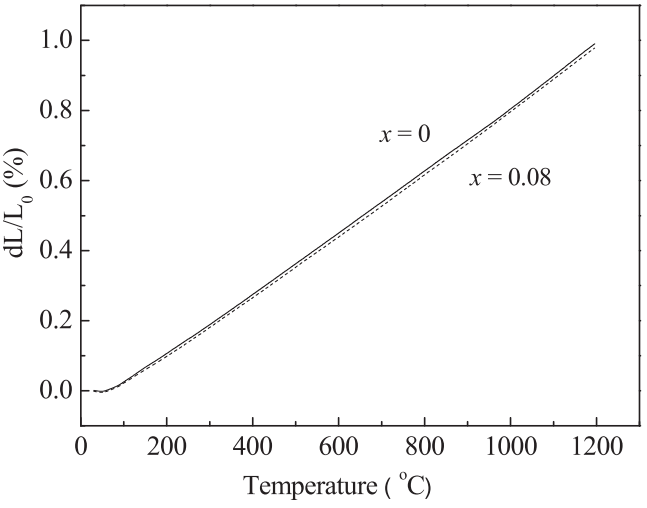

Fig. 5. Calibrated dilatometric data of $LaMgAl_{11}O_{19}$–$Yb_3Al_5O_{12}$ ceramic composites as a function of temperature.

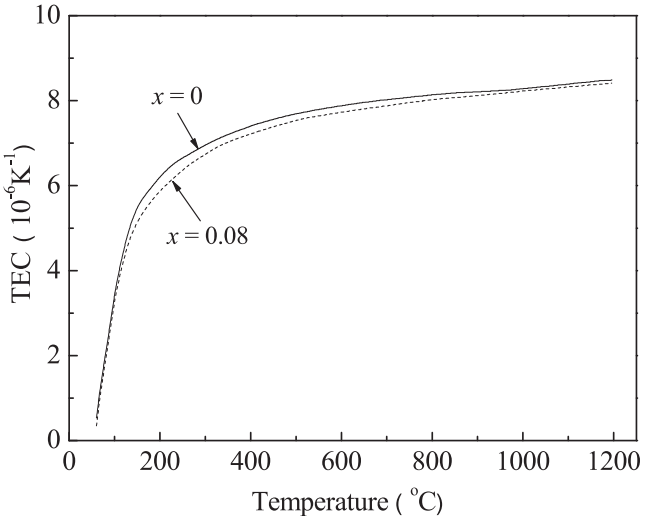

Fig. 6. Thermal expansion coefficient of $LaMgAl_{11}O_{19}$–$Yb_3Al_5O_{12}$ ceramic composites as a function of temperature.

Fig. 4. The error bars are omitted as they are smaller than the symbols. It can be seen that the thermal conductivity of $LaMgAl_{11}O_{19}$–$Yb_3Al_5O_{12}$ ceramic composites is in the range of 2.6–3.9 $W \cdot m^{-1} \cdot K^{-1}$ from room temperature to 1200 °C.

Thermal expansion coefficient is an important property for the TBCs applications. The results of the dilatometric measurements for selected $LaMgAl_{11}O_{19}$–$Yb_3Al_5O_{12}$ ceramic composites with calibration are shown in Fig. 5. The thermal expansion shows typical linear increase with increasing temperature from room temperature to 1200 °C, which is a typical characteristic of solid materials. From the dilatometric data, no phase transformation coupled with a drastic change of volume or thermal expansion coefficient takes place during heating. Therefore it is favorable for TBCs application. Fig. 6 presents the thermal expansion coefficient of $LaMgAl_{11}O_{19}$–$Yb_3Al_5O_{12}$ ceramics. The thermal expansion coefficient of $LaMgAl_{11}O_{19}$ and $0.92LaMgAl_{11}O_{19}$–$0.08Yb_3Al_5O_{12}$ are $8.49 \times 10^{-6}\,K^{-1}$ and $8.41 \times 10^{-6}\,K^{-1}$ at 1200 °C, respectively. At identical temperature levels, thermal expansion coefficient of $0.92LaMgAl_{11}O_{19}$–$0.08Yb_3Al_5O_{12}$ is slightly lower than that of pure $LaMgAl_{11}O_{19}$, which can be seen from both Figs. 5 and 6.

4. Conclusions

$LaMgAl_{11}O_{19}$–$Yb_3Al_5O_{12}$ ceramic composites sintered at 1700 °C for 10 h are composed of both magnetoplumbite and garnet structures. The composites exhibit typical linear increase in thermal expansion with the increase of temperature. The thermal expansion coefficients of $LaMgAl_{11}O_{19}$ and $0.92LaMgAl_{11}O_{19}$–$0.08Yb_3Al_5O_{12}$ are $8.49 \times 10^{-6}\,K^{-1}$ and $8.41 \times 10^{-6}\,K^{-1}$ at 1200 °C, respectively. The measured thermal diffusivity decreases gradually with increasing temperature. Thermal conductivity of the composites is in the range of 2.6–3.9 $W \cdot m^{-1} \cdot K^{-1}$ from room temperature to 1200 °C.

Acknowledgements

This work was partially supported by the National Natural Science Foundation of China (NSFC-Nos. 51002038 and 51021002), and the Fundamental Research Funds for the Central Universities (Grant No. HIT.BRET1.2010006).

References

[1] N.P. Padture, M. Gell, E.H. Jordan, Thermal barrier coatings for gas-turbine engine applications, Science 296 (2002) 280–284.
[2] C.G. Levi, Emerging materials and processes for thermal barrier systems, Curr. Opin. Solid State Mater. Sci. 8 (1) (2004) 77–91.
[3] D.R. Clarke, S.R. Phillpot, Thermal barrier coating materials, Mater. Today 8 (6) (2005) 22–29.
[4] S.Q. Guo, Y. Kagawa, Isothermal and cycle properties of EB-PVD yttria-partially-stabilized zirconia thermal barrier coatings at 1150 and 1300 °C, Ceram. Int. 33 (3) (2007) 373–378.
[5] Z.-G. Liu, J.-H. Ouyang, Y. Zhou, Influence of gadolinia on thermal expansion property of ZrO_2-4.5 mol%Y_2O_3 ceramics, J. Alloys Compd. 473 (1–2) (2009) L17–L19.
[6] G. Di Girolamo, C. Blasi, M. Schioppa, L. Tapfer, Structure and thermal properties of heat treated plasma sprayed ceria yttria co-stabilized zirconia coatings, Ceram. Int. 36 (3) (2010) 961–968.
[7] D.M. Zhu, R.A. Miller, Development of advanced low conductivity thermal barrier coatings, Int. J. Appl. Ceram. Technol. 1 (1) (2004) 86–94.
[8] J. Wu, X.Z. Wei, N.P. Padture, P.G. Klemens, M. Gell, E. Garcia, P. Miranzo, M.I. Osendi, Low-thermal-conductivity rare-earth zirconates for potential thermal-barrier-coating applications, J. Am. Ceram. Soc. 85 (12) (2002) 3031–3035.
[9] C. Friedrich, R. Gadow, T. Schirmer, Lanthanum hexaluminate-a new material for atmospheric plasma spraying of advanced thermal barrier coatings, J. Therm. Spray. Technol. 10 (4) (2001) 592–598.
[10] R. Gadow, M. Lischka, Lanthanum hexaaluminate–novel thermal barrier coatings for gas turbine applications–materials and process development, Surf. Coat. Techonl. 151–152 (2002) 392–399.
[11] G.W. Schafer, R. Gadow, Lanthane aluminate thermal barrier coating, Ceram. Eng. Sci. Proc. 20 (4) (1999) 291–297.
[12] N.P. Bansal, D.M. Zhu, Thermal properties of oxides with magnetoplumbite structure for advanced thermal barrier coatings, Surf. Coat. Techonl. 202 (12) (2008) 2698–2703.
[13] J.R. Nicholls, K.J. Lawson, A. Johnstone, D.S. Rickerby, Methods to reduce the thermal conductivity of EB–PVD TBCs, Surf. Coat. Techonl. 151–152 (2002) 383–391.
[14] Z.-G. Liu, J.-H. Ouyang, Y. Zhou, Effect of gadolinia on phase structure and thermal conductivity of ZrO_2-4.5mol% Y_2O_3 ceramics, Mater. Lett. 62 (20) (2008) 3524–3526.
[15] Z.-G. Liu, J.-H. Ouyang, Y. Zhou, Preparation and thermophysical properties of $(Nd_xGd_{1-x})_2Zr_2O_7$ ceramics, J. Mater. Sci. 43 (10) (2008) 3596–3603.
[16] Z.-G. Liu, J.-H. Ouyang, Y. Zhou, J. Li, X.-L. Xia, Densification, structure and thermophysical properties of ytterbium–gadolinium zirconate ceramics, Int. J. Appl. Ceram. Technol. 6 (4) (2009) 485–491.
[17] Z.-G. Liu, J.-H. Ouyang, Y. Zhou, Q.-C. Meng, X.-L. Xia, Order–disorder transition and thermal conductivity of $(Yb_xNd_{1-x})_2Zr_2O_7$ solid solutions, Philos. Mag. 89 (6) (2009) 553–564.
[18] R.A. Swalin, Thermodynamics of Solids, second ed., John Wiley & Sons, New York, 1972, 53-87.
[19] O. Kubaschewsji, C.B. Alcock, P.J. Spencer, Materials Thermochemistry, sixth ed., Pergamon Press, Oxford, 1993, 257-323.
[20] R. Berman, Thermal Conduction in Solids., Clarendon Press, Oxford, 1976, 45-101.